

Underwater sound transmission through arrays of disk cavities in a soft elastic medium

David C. Calvo,^{a)} Abel L. Thangawng, and Christopher N. Layman, Jr.
Acoustics Division, Naval Research Laboratory, Code 7165, 4555 Overlook Avenue SW, Washington, DC 20375, USA

Riccardo Casalini
Chemistry Division, Naval Research Laboratory, Code 6126, 4555 Overlook Avenue SW, Washington, DC 20375, USA

Shadi F. Othman
Department of Biological Systems Engineering, University of Nebraska-Lincoln, 233 L. W. Chase Hall, Lincoln, Nebraska 68583, USA

(Received 20 October 2014; revised 6 August 2015; accepted 9 September 2015; published online 29 October 2015)

Scattering from a cavity in a soft elastic medium, such as silicone rubber, resembles scattering from an underwater bubble in that low-frequency monopole resonance is obtainable in both cases. Arrays of cavities can therefore be used to reduce underwater sound transmission using thin layers and low void fractions. This article examines the role of cavity shape by microfabricating arrays of disk-shaped air cavities into single and multiple layers of polydimethylsiloxane. Comparison is made with the case of equivalent volume cylinders which approximate spheres. Measurements of ultrasonic underwater sound transmission are compared with finite element modeling predictions. The disks provide a deeper transmission minimum at a lower frequency owing to the drum-type breathing resonance. The resonance of a single disk cavity in an unbounded medium is also calculated and compared with a derived estimate of the natural frequency of the drum mode. Variation of transmission is determined as a function of disk tilt angle, lattice constant, and layer thickness. A modeled transmission loss of 18 dB can be obtained at a wavelength about 20 times the three-layer thickness, and thinner results (wavelength/thickness ~ 240) are possible for the same loss with a single layer depending on allowable hydrostatic pressure.

[<http://dx.doi.org/10.1121/1.4931446>]

[DF]

Pages: 2537–2547

I. INTRODUCTION

The scattering and radiation of waves by a spherical cavity in an elastic medium has been studied by multiple efforts in the acoustics literature.^{1–5} Early work⁶ identified that monopole resonance is obtained when the circumference of the cavity equals twice the shear wavelength. For soft elastic media, such as silicone rubber, the shear wave speed is typically two orders of magnitude smaller than the compression wave speed and therefore long-wavelength acoustic resonance is obtained much like the Minnaert resonance of a gas bubble in a liquid.⁷ There has been renewed interest in monopole resonant scattering in soft media for experimental studies of phononic crystals and phenomena associated with random distributions of scatterers.^{8–10}

The influence of cavity shape on natural frequency was studied in Meyer *et al.*⁶ where a variety of shapes molded into rubber were examined experimentally. Deviations from spherical predictions were noticed for large aspect ratio (AR) shapes as also found in Ivansson.¹¹ Recent numerical work¹² has shown that the monopole resonance frequency of an evacuated sphere in a soft medium can be reduced by a

factor of up to 6 by distorting the shape into a high AR oblate spheroid keeping the volume constant. The presence of air was found to have a stiffening effect, raising the resonance frequency for both shapes, although the shear modulus is typically large enough that air is a secondary factor.

The present study focuses on the computation and ultrasonic measurement of underwater sound transmission through single and multiple planar arrays of disk-shaped cavities molded into layers of silicone rubber [polydimethylsiloxane (PDMS)]. The objective is to reduce transmission using relatively thin material layers. Such patterned layers, when scaled appropriately, have potential use in applications such as underwater noise abatement.¹³ In previous work, the disk cavity is referred to as a penny-shaped crack or a pancake shape.^{12,14–16} Although a single layer of what is considered resembles the arrays studied in the context of Alberich underwater anechoic coatings,^{11,17,18} this study is distinct in examining large AR disk cavities in both single- and multi-layered geometries with both sides exposed to water. At the ultrasonic frequencies considered (>50 kHz), the shear loss factor of PDMS is large, which affects the quality of the resonance of an individual cavity. Nevertheless, an array of cavities creates significant transmission reduction even for a single layer due to coherent superposition of scattering from all elements in the array and their mutual interaction.¹⁹

^{a)}Electronic mail: david.calvo@nrl.navy.mil

The study is organized as follows. In Sec. II, the resonance frequency for pulsation of a single disk cavity in unbounded PDMS is computed as a baseline using the finite element method and compared with a derived estimate. Differences from an equivalent volume spherical cavity are highlighted. In Sec. III, the geometry of the array is described along with the numerical model, fabrication technique, and underwater acoustic measurements. Transmission measurements are compared with numerical predictions. An analysis of the relative contribution of reflection and absorption to the transmission loss is presented in Sec. IV. In Sec. V, transmission sensitivity to disk orientation, layer thickness, and lattice constant changes are examined, followed by conclusions in Sec. VI.

II. RESONANCE OF A SINGLE DISK CAVITY

The monopole resonance frequency of a single disk cavity in an unbounded soft elastic medium is first computed as a baseline to compare with the subsequent array case in which neighboring disks affect the resonance frequency. For comparison and validation purposes, the scattering amplitude of an air-filled spherical cavity of equivalent volume is also considered.

A. Numerical model

The geometry of a single cavity is depicted in Fig. 1(a). A unit amplitude longitudinal wave is incident in the axial (z) direction. Because the cavity is assumed small in comparison with the incident wavelengths considered, it experiences an essentially uniform oscillatory pressure.⁵ The associated radiation problem is therefore solved where a unit amplitude boundary pressure load $p_0 = 1$ Pa is applied to the interior surfaces of the cavity. This approach provides computational simplicity in the finite element framework used to model elastic wave propagation (COMSOL Multiphysics).²⁰ The problem is formulated as an acoustic–solid interaction in an axisymmetric geometry. The simplified geometry, subdomains, and boundary conditions are shown in Fig. 1(b). Because of the focus on monopole resonance, further computational simplification is possible by modeling only $z > 0$.¹² The boundary condition on $z = 0$ for the solid is no z -component of the displacement and no shear stresses (roller condition).

A disk cavity of diameter $D = 120 \mu\text{m}$ and height $h = 5 \mu\text{m}$ is modeled, which corresponds to the size of the fabricated cavities in Sec. III. The AR is defined as D/h (AR = 24 for the disk). In reference to Fig. 1(b) (not to scale), a computational domain for the PDMS of 1 mm radius is used, which terminates at a standard perfectly matched layer (PML) of 14 mm thickness. This thickness is sufficient to absorb long compression and short shear waves. The maximum adequate mesh element size (obtained through a convergence analysis) gradually increases with radius from $1 \mu\text{m}$ inside the cavity, $10 \mu\text{m}$ in the PDMS (sufficient to resolve the shear waves over the frequencies considered), and 1 mm in the PML. Since Poisson’s ratio is close to $\frac{1}{2}$, a formulation²⁰ for a nearly incompressible medium is used, which stably computes a pressure field

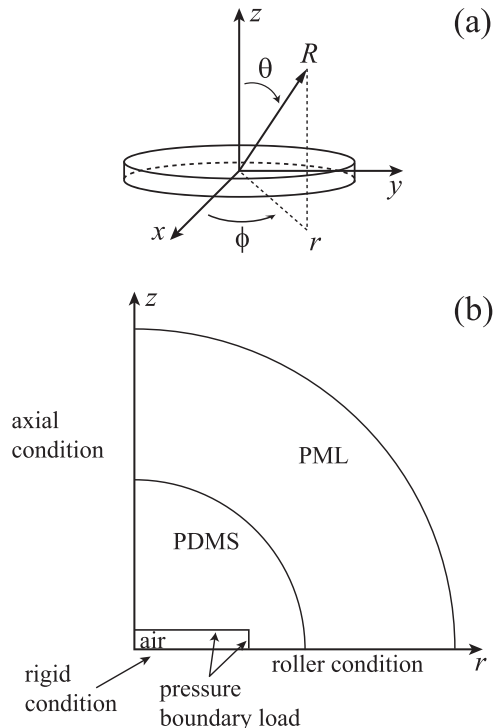


FIG. 1. (a) Coordinate system with origin at the cavity center for the single-cavity case. (b) Schematic (not to scale) of the computational domain and boundary conditions used to model long-wavelength scattering/radiation from the cavity (air-filled case depicted). The displacement field is axisymmetric about the z axis and antisymmetric about $z = 0$.

from which the scattering amplitude is determined. The pressure in an elastic medium is defined as the negative of the bulk modulus times the dilatation (volumetric strain). Equivalently, the pressure is the negative of the average normal stress.²¹ For a nearly incompressible elastic medium, the normal stress tensor components are approximately equal. The numerical model was checked by computing the total scattering cross section of an oblate spheroidal cavity of AR 2 in a non-viscous medium as reported in Ref. 11.

The material parameters in this section typify the ultrasonic characteristics of PDMS discussed in Sec. III, but frequency dependence is here neglected (it is included in the subsequent array computations). A shear storage modulus of $\mu' = 946$ kPa is used (typical near 200 kHz). The density of a 10:1 (monomer:hardener) mixture of RTV-615 (Momentive, Columbus, OH) PDMS is $\rho = 1040$ kg/m³. The shear wave speed is therefore $c_s = 30.2$ m/s. The P -wave modulus (M) is related to the compression wave speed of $c_p = 1049$ m/s by $M = \rho c_p^2$. An air density of $\rho_a = 1.2$ kg/m³ and a sound speed of $c_a = 343$ m/s are assumed. We note that in computations for a nearly incompressible medium, if the Young’s modulus E and Poisson ratio ν are specified as elastic constants, ν must be specified with relatively high precision to avoid large errors in the compression wave speed.

B. Scattering amplitude

The monopole scattering amplitude F for compression waves is related to the scattered pressure p_{sc} by

$$p_{sc} = p_0 \frac{F}{R} e^{i(k_p R - 2\pi f t)}, \quad (1)$$

where R is the propagation distance, f is the frequency, and $k_p = 2\pi f/c_p$ is the wavenumber. For comparison and validation purposes, the scattering amplitude for an air-filled spherical cavity is calculated along with the disk case. For a spherical cavity of radius a , an exact expression can be derived⁵

$$F = \frac{a}{\left(\frac{f_0}{f}\right)^2 - 1 - i\delta}, \quad (2)$$

where f_0 is the resonance frequency and δ is the damping factor, which is generally a sum of radiation, viscous, and thermal losses. The radiation damping loss is $\delta_{\text{rad}} = k_p a$ and the viscous loss is $\delta_{\text{vis}} = 4\mu''/\rho a^2 (2\pi f)^2$ where μ'' is the imaginary part of the shear modulus. For the cavity sizes and frequencies considered, computations showed that thermal losses are weak in comparison with radiation and viscous losses. The monopole resonance frequency is then given by

$$f_0 = \frac{1}{2\pi a} \left(\frac{3\rho_a c_a^2 + 4\mu'}{\rho} \right)^{1/2}, \quad (3)$$

where μ' is the real part of the shear modulus. This expression reduces to the Minnaert frequency of an air bubble in a liquid when μ' vanishes. The shear modulus for PDMS is such that $\mu' \ll M$ and $\mu' \gg 3\rho_a c_a^2/4$. The medium is therefore soft enough that low-frequency resonance can be obtained yet stiff enough that the deformation is elastic dominated in contrast to an air bubble in a liquid.

C. Results

Results are presented first for an air-filled spherical cavity of radius $a = 23.8 \mu\text{m}$, which has the same volume as the disk. The scattering amplitude F is computed by evaluating Eq. (1) over increasingly large radial arcs in the PDMS computational domain until the scaling relationship is accurate and F is omni-directional. Values of F are plotted in Fig. 2(a) which shows the resonance frequency obtained at 425 kHz in agreement with the analytical result (curves overlap). The analytical scattering amplitude including viscous effects ($\mu'' = 0.7\mu' = 662 \text{ kPa}$) is also plotted and shows the strong importance of viscosity in this frequency regime, which is accounted for in the array calculations in Sec. III. Both air-filled and evacuated disk cavity scattering amplitudes are also shown with viscous loss neglected. Two displacement components that generally comprise the monopole resonance of a finite-length cylindrical cavity are an opposing drum-like mode of the top and bottom interfaces and a radial pulsation of the side walls.^{17,18,22–25} For a disk (a short cylinder), the monopole mode is predominantly the drum mode. Snapshots of an animation of the drum mode are displayed in Fig. 3 for the symmetric geometry. Plots of the scattering amplitude in Fig. 2(a) show the evacuated disk cavity obtains this resonance at 163 kHz and the air-filled cavity at 242 kHz. The

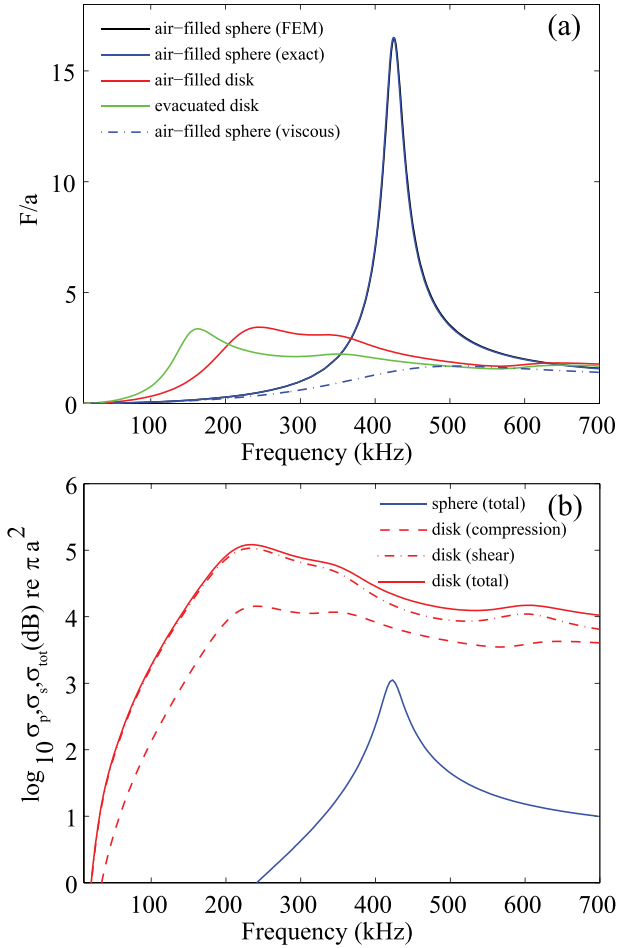


FIG. 2. (Color online) (a) Comparison of the scattered pressure monopole amplitude (F) for the air-filled sphere, evacuated disk, and air-filled disk cavities. The incident field is a unit amplitude P-wave along the z axis. (b) Scattering cross sections for the sphere and disk cases (compression, shear, total). In the sphere case, the scattered field is entirely a compression wave in the low-frequency approximation made. Viscous loss is neglected unless noted.

slight resonance detectable at 350 kHz in Fig. 2(a) (in both evacuated and air-filled disk cases) corresponds to the drum resonance being in a higher mode of vibration in which the air has little effect on the mode shape.

Compression and shear wave scattering cross sections can be calculated based on the scattered elastic displacement field, which in the far-field ($k_p R \gg 1$) is generally given by^{26,27}

$$\vec{u}_{sc}(\theta, \phi, R) = u_0 \left[A(\theta, \phi) \frac{e^{ik_p R}}{R} \hat{R} + B(\theta, \phi) \frac{e^{ik_s R}}{R} \hat{\theta} \right], \quad (4)$$

where $u_0 = p_0/2\pi f \rho c_p$ is the incident longitudinal wave displacement amplitude corresponding to the compressive stress amplitude p_0 . The scattering amplitudes A and B correspond to longitudinal (p) and transverse (s) waves, respectively. Similar to before, A and B are extracted from the finite element simulated displacement field at a sufficient radial distance in which the scaling in Eq. (4) becomes accurate. Numerical refinement tests showed that excessive gridding out to many compression wavelengths was not required since the cavity radiates compression waves like a

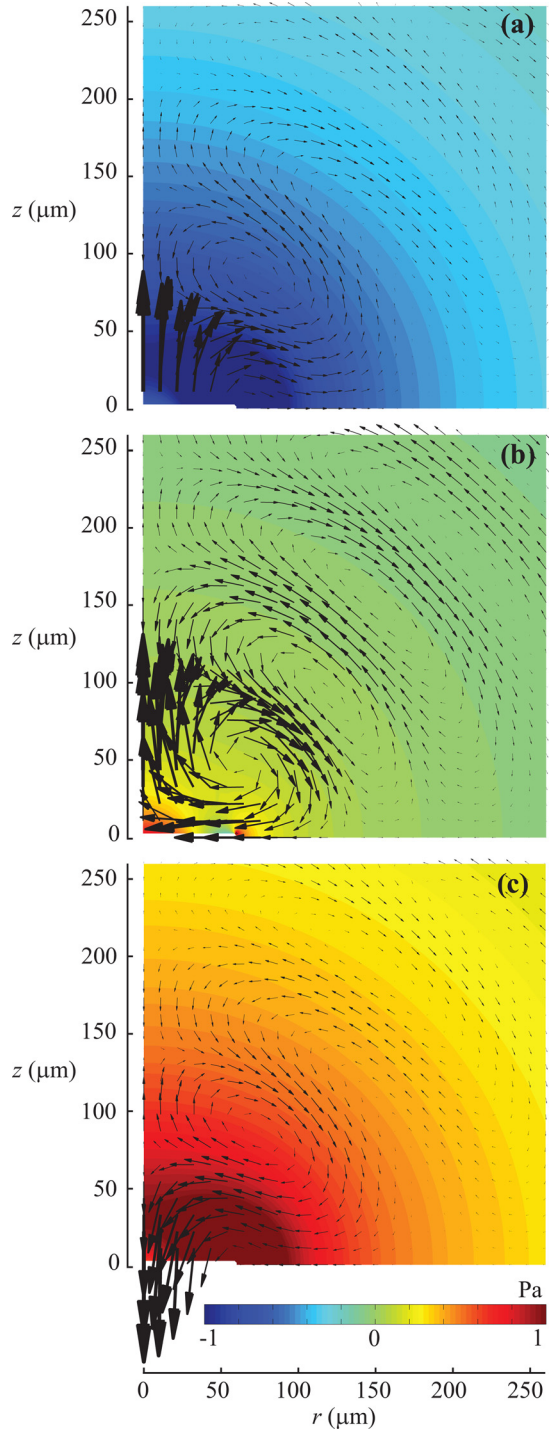


FIG. 3. (Color online) Animation snapshots of the breathing oscillation of a single air-filled disk cavity forced by a unit-amplitude time harmonic (242 kHz) boundary pressure load on the interior surfaces. The vector displacement field and pressure are plotted in the solid. Snapshots are created by advancing the solution phase by (a) 1.89 rad, (b) 3.46 rad, and (c) 5.03 rad to show the maximum excursion instants centered about the middle instant of zero radiated pressure. Generation of shear waves that radiate in the $\theta = \pi/4$ direction is evident. The pressure field of the air inside the cavity is not displayed.

compact monopole. The differential scattering cross sections specific to the incident longitudinal wave case are given by²⁶

$$\frac{d\sigma_p}{d\Omega} = |A|^2, \quad (5a)$$

$$\frac{d\sigma_s}{d\Omega} = \frac{k_p}{k_s} |B|^2. \quad (5b)$$

The scattering cross sections are obtained by integrating Eqs. (5a) and (5b) over 4π steradians in the set of spherical coordinates $\Omega = (\theta, \phi)$ while taking into account symmetries in the computation. The total scattering cross section in the absence of absorption is $\sigma_{\text{tot}} = \sigma_p + \sigma_s$.¹⁶ Results in Fig. 2(b) show that the energy scattered to the far-field in the disk case is mainly conveyed by shear waves. The difference in the quality factors of the compression wave scattering amplitudes in Fig. 2(a) can therefore be attributed to shear wave radiation loss that is absent in the spherical case due to symmetry of the geometry and the assumed symmetry of the forcing (reasonable in a long-wavelength approximation). This effect can be visualized in Fig. 3 in which the displacement field, shown at three different phase instants, is a combination of disk pulsation and generation of shear waves by a vortex near the cavity. The neglect of attenuation allows a clear visualization of the shearing part of displacement field although in practice these shear waves are rapidly absorbed due to the viscosity of rubber. The pressure field is also plotted to correlate with the breathing motion of the cavity. It is important to note that in the absence of shear wave generation, absorption can still be significant, in general, owing to the extensional strains near the cavity surface as is the case of the hoop-stress around a spherical cavity. A complete analysis of absorption is beyond the scope of this study, although the relative contribution of absorption to transmission reduction is analyzed in Sec. IV for the array problem.

D. Estimate of natural frequency

An estimate of the natural pulsation frequency of the disk cavity can be made in the low-frequency limit by modeling the stiffness of the cavity and estimating the radiation mass. It is sufficient to analyze $z > 0$ given the symmetry of the problem. The interface stiffness, specifically the force required to achieve an average displacement of the interface, can be obtained from the classical elasticity expression derived by Sneddon¹⁴ for the normal displacement w as a function of radius r on the circular face of a penny-shaped crack where a uniform internal pressure p_0 is applied

$$w(r) = \frac{4p_0(1-\nu^2)}{\pi E} \left(\frac{D^2}{4} - r^2 \right)^{1/2}. \quad (6)$$

The Poisson ratio (ν) and Young's modulus (E) are related to the wave speeds and density by $\nu = (1 - 2c_s^2/c_p^2)/(2 - 2c_s^2/c_p^2)$ and $E = \rho c_p^2(1 + \nu)(1 - 2\nu)/(1 - \nu)$. Straightforward analysis shows that the interface stiffness is given by

$$k_{\text{int}} = \frac{3}{16} \frac{\pi^2 E}{(1 - \nu^2)} D. \quad (7)$$

Similar analysis shows that the air spring located in $z > 0$ has a stiffness of

$$k_a = \frac{\pi D^2}{2h} \rho_a c_a^2. \quad (8)$$

Although the elastic displacement field in Fig. 3 is complex, axial displacements in close proximity to the interface are relatively large, and so a simple acoustic estimate of the radiation mass m_{rad} of a baffled piston is invoked²⁸

$$m_{\text{rad}} = \frac{1}{3} \rho D^3. \quad (9)$$

An expression for the natural frequency of the air-filled disk is given by $f_{afd} = [(k_{\text{int}} + k_a)/m_{\text{rad}}]^{1/2}/2\pi$,

$$f_{afd} = \frac{1}{4D} \sqrt{\frac{9}{4} \frac{E}{\rho(1-\nu^2)} + \frac{6D\rho_a c_a^2}{\pi\rho h}}. \quad (10)$$

For the evacuated cavity ($\rho_a=0$) a value of 189 kHz is obtained in reasonable agreement with the finite element resonant peak value of 163 kHz (16% deviation). In the air-filled case, the estimate is 250 kHz compared to the finite element value of 242 kHz (3.3% deviation). In each case, the natural frequency prediction is greater than the resonant peak amplitude frequencies, which is consistent with a damped mass-spring oscillator obtaining its resonance at the damped natural frequency, which is lower than the natural frequency. Despite the approximate nature of Eq. (10), comparison with finite element results showed that scaling with inverse diameter is valid and the evacuated case showed weak dependence on cavity height provided the AR is ten or above. The estimate is only expected to be valid if the Young's modulus is on the order or greater than the bulk modulus of the air as it does not reduce to the natural frequency of a disk air bubble in the limit of vanishing shear modulus. A more rigorous analysis would be required to improve accuracy and allow for uniform behavior between solid and fluid limits of the host.

III. TRANSMISSION THROUGH ARRAYS OF DISK CAVITIES

Arrays of disk cavities, both single and multi-layered, are examined both experimentally and numerically for usefulness in blocking sound with wavelengths much longer than the overall layer thickness. Of particular interest is determining how cavity shape affects transmission.

A. Geometry and finite element model

Schematics of the array geometry considered are shown in Figs. 4(a) and 4(b). The disk cavities again have diameter $120 \mu\text{m}$ and height $5 \mu\text{m}$. With reference to the fabrication technique that will be described later, the fundamental single-layer geometry consists of a single horizontal square array of disk cavities of lattice constant $d=300 \mu\text{m}$ patterned into the top of a PDMS layer of thickness d_z . An unpatterned PDMS cover layer is then bonded to the top of this layer. The sealed layer is then bonded to additional patterned layers. Each layer has the same thickness

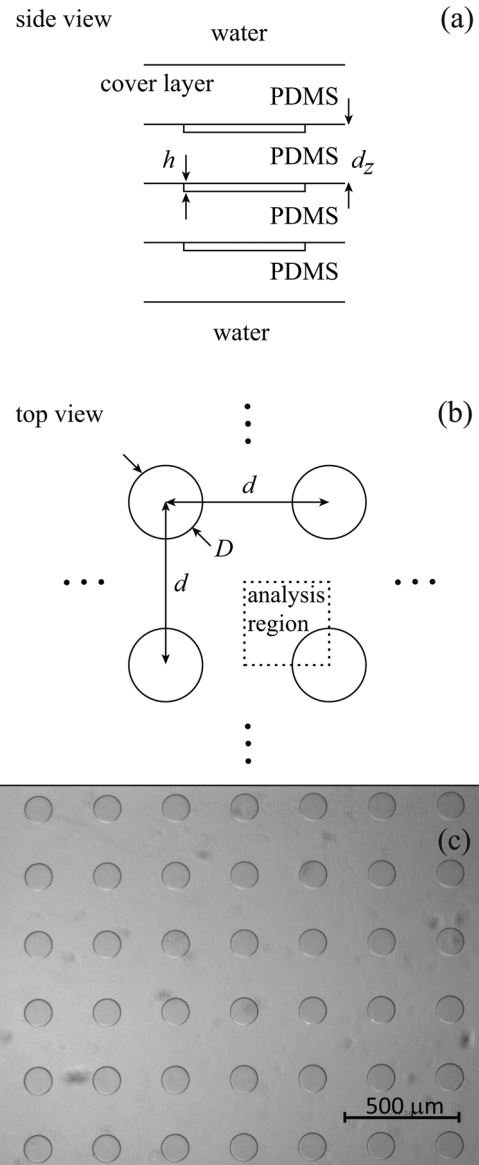


FIG. 4. (a) Geometry of air-filled disk cavities in PDMS layers (three-layer case shown; not to scale). (b) The finite element analysis region for normal incidence is shown relative to the lattice spacing. (c) Image of a single fabricated layer of disk cavities.

$d_z = 375 \mu\text{m}$ giving the three-layer geometry an overall thickness of 1.5 mm.

Only normal sound wave incidence is examined, which allows a great deal of simplification of the computational geometry due to symmetry.²⁵ The finite element analysis region consists of a quarter unit cell [Fig. 4(b)] in which the boundary conditions applied are depicted in Fig. 5. The computation is formulated as a scattering problem in which a normally incident plane wave is present in the water and radiation boundary conditions are applied at the outermost axial water boundaries. The sound speed and density in water is 1482 m/s and 1000 kg/m^3 , respectively.

The finite element mesh used a minimum of six elements per shear wavelength in the regions surrounding the disk inclusions shown in Fig. 5 where radiation and damping of shear waves are expected. Because the shear loss factor in PDMS is large at the frequencies considered, the

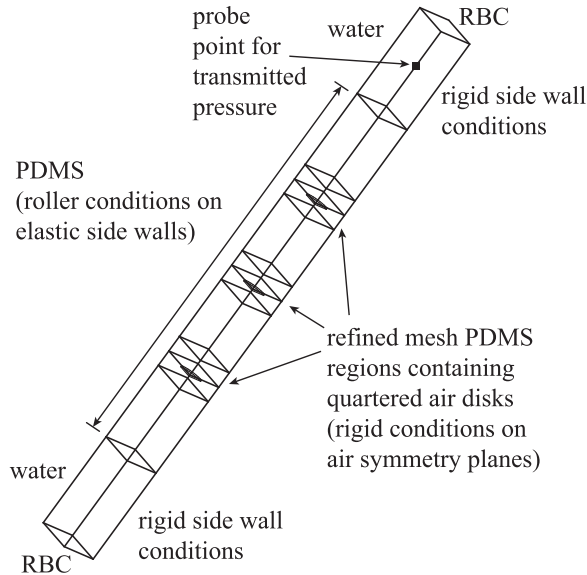


FIG. 5. Axial profile of the finite element analysis region for the three-layer case indicating boundary conditions for normal sound wave incidence. Regions of higher mesh refinement to accurately resolve shear waves are indicated.

mesh was relaxed to a minimum of four elements per shear wavelength in the neighboring PDMS regions where the shear stress amplitudes are naturally lower. In the water, the mesh was twice as coarse as the outer PDMS mesh. These mesh sizes were found to be sufficient by performing mesh refinement studies at selected high-end frequencies in the results.

B. Sample fabrication and acoustic measurements

Test sample dimensions were selected to minimize diffraction around the edges of the overall array sample given the ultrasonic immersion transducers used and the size constraints on fabrication equipment. The PDMS used in the experiments is RTV-615 (Momentive, Columbus, OH) mixed with a standard 10:1 monomer to hardener ratio. A laser pattern generator (DWL66, Heidelberg Instruments, Germany) was used to create a mask that was then used in a photolithography process to create an SU-8 mold. The patterned area was 3×3 in.². The mold was filled with mixed liquid PDMS, spin-coated to the desired thickness of $375 \mu\text{m}$ and then degassed and cured at 70°C for 1 h. Layers were bonded together using a plasma oxidation treatment (SURFX Technologies, Redondo Beach, CA). An image of a single-layer array of disk cavities is shown in Fig. 4(c). Perfect alignment of multiple array layers was not obtained, as was the case in previous soft medium sonic crystal work,⁹ although for normal incidence this does not appear to be a major limitation.

Experimental data were separately collected using two pairs of broadband immersion transducers driven by a pulser (Models V301, V303, and 5077PR, Olympus, Waltham, MA). One pair (V301) operated at a center frequency of 0.5 MHz with an active element diameter of 1 in. The other pair (V303) operated at a center frequency of 1 MHz with an

active element diameter of 0.5 in. In each pair, one element operated as a source and the other as a receiver in a through-transmission configuration. The pulser excited the sources with a short broadband pulse and the received signal was sent to a digital oscilloscope (Lecroy Wavesurfer 424, Teledyne LeCroy, Chestnut Ridge, NY) and saved. Both the source and receiver were positioned ~ 10 cm from the sample faces (in the far-field). The transmission coefficient was computed as a ratio of Fourier transforms

$$T = 20 \log_{10} \left| \frac{P_{\text{trans}}(f)}{P_{\text{inc}}(f)} \right|, \quad (11)$$

where P_{trans} is the transform of the time-gated first arrival with the sample present and P_{inc} is with the sample absent. In the simulations, transmission was sampled at the probe location in Fig. 5.

Computations used a frequency-dependent viscoelastic shear modulus and compression wave attenuation. Shear moduli for RTV-615 have been reported in Ref. 10 based on a shear wave reflection technique.²⁹ The following fit is reported for the shear storage (μ') and loss (μ'') moduli in the range $30 < f < 500$ kHz:

$$\mu' = 0.6 + 0.7f, \quad (12a)$$

$$\mu'' = 0.2 + 1.8f, \quad (12b)$$

where the moduli are in MPa and the frequency is in MHz. Additionally, a low-frequency shear modulus measurement was made in the present study using the magnetic resonance elastography (MRE) method³⁰ at 1095 Hz. The MRE loss factor μ''/μ' agreed with the fit derived from Eq. (12) extrapolated to the measurement frequency.

The compression wave speed and attenuation of unpatterned PDMS were measured in a similar through-transmission geometry as described before. After time gating the first clear arrival through the sample, the broadband substitution (spectral ratio) method of extracting the phase speed and attenuation was used.³¹ A power-law fit of the compression wave attenuation over 300–700 kHz was measured to be

$$\alpha = 0.0186f^{2.04}, \quad (13)$$

where α is in nepers/mm and f is in MHz. The compression wave speed was measured to be $c_p = 1049$ m/s with only slight dispersion in the bandwidth considered consistent with the relatively low compression wave attenuation.

C. Results for array geometries

Comparisons begin by examining the transmission difference between two single-layer arrays: one with disk cavities ($AR=24$) and the other with equivalent volume cylindrical cavities, also fabricated, of diameter and height both equal to $41.6 \mu\text{m}$ ($AR=1$) to approximate spheres.⁹ The lattice constant is the same in both cases.

Results for these single-layer cases are presented in Fig. 6. The finite element results agree well with the

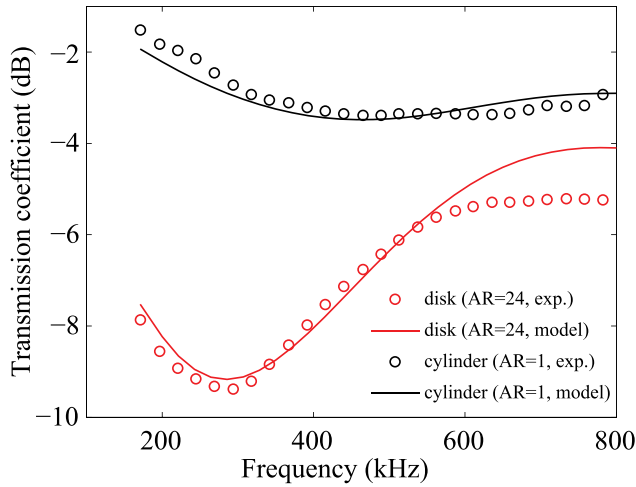


FIG. 6. (Color online) Comparison of measured vs calculated transmission coefficients for single-layer arrays of cavities. Volumes of disk and cylinder cavities are equivalent. Lattice constant is the same in both cases.

measured points. The disk cavities create a larger transmission loss at a lower frequency compared with the use of approximate spheres. The degree to which reflection vs absorption contributes to the transmission loss will be examined in Sec. IV. The shallow minimum for the approximate sphere case is obtained at 470 kHz (modeled), which is greater than the single-cavity 425 kHz free-field value. Resonant transmission reduction through a single-layer array of spherical air bubbles in a gel was studied by Leroy *et al.*¹⁹ Interestingly, the transmission minimum occurred at a frequency higher than the Minnaert frequency. The increase is attributed to self-consistent or mutual scattering effects that become important as the separation between the scatterers decreases. A similar effect was found for a single-layer array of approximate sphere cavities in PDMS.⁹ For our disk cavities, a transmission minimum is found at 287 kHz, which is similarly greater than the free-field resonant scattering value of 242 kHz. Our disk cavity resonance shift is therefore qualitatively similar to that discussed in Leroy *et al.*¹⁹

Results for multiple layers of disk cavities are shown in Fig. 7. Measured transmission loss is largest with three layers reaching a maximum of 27 dB at 400 kHz. Examination of the modeled displacement field showed the cavities to be in monopole resonance at the minimum of each curve. Agreement with computations is good overall with the three-layer case developing a first-order Bragg diffraction local minimum near 1.4 MHz in agreement with Bragg theory ($f = c_p/2d_z$) given the compression wave speed in PDMS and the z -separation of the cavities. It is noted that the dip in transmission in the single-layer case near 1.2 MHz is caused by a higher-order resonance of the disk array in which the breathing deflection of each cavity is largest near the perimeter and not the center. The experimental results were obtained using the wideband transducer centered at 1 MHz, which allowed probing near 3 MHz owing to a strong third harmonic. Data obtained using the 500 kHz source over its full bandwidth overlapped the corresponding subset of data taken using

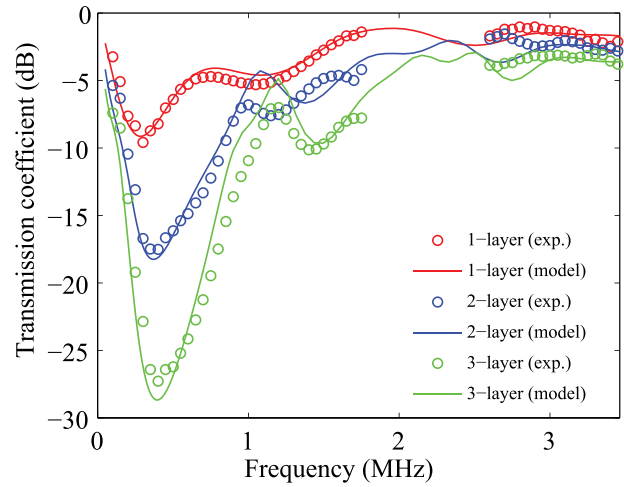


FIG. 7. (Color online) Transmission through multiple layers of disk cavity arrays. Both numerically modeled and experimental results are compared.

the 1 MHz source, but are omitted for graphical clarity in Fig. 7.

To draw more distinction between the disk and equivalent volume approximate-sphere results, computations for three-layer cases are shown in Fig. 8. Both cases have the same lattice constant and therefore the gas volume fraction is the same in both samples (0.168% assuming a lattice continuing in the z -direction). As in the single-layer case, the disks provide a higher transmission loss at a lower frequency compared to the approximate spheres for equivalent volume.

Modeled transmission through the same three-layer system but with no cavities is also shown with and without absorption as a reference. The low amplitude oscillation in transmission with frequency $\Delta f = c_p/2d_{\text{tot}} = 0.35$ MHz is caused by Fabry-Pérot effects³² in the $d_{\text{tot}} = 4d_z = 1.5$ mm total thickness layer, which has a compression wave speed that differs from water (1049 m/s vs 1482 m/s). The unpatterned layer is nearly transparent below 1 MHz.

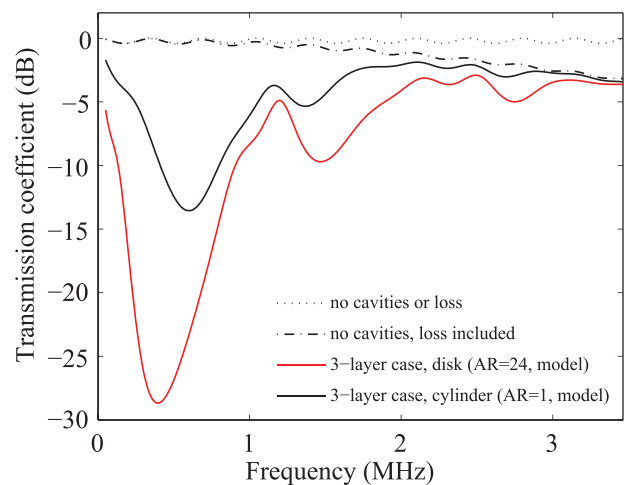


FIG. 8. Modeled transmission through three-layer arrays of disks and equivalent volume approximate spheres (i.e., cylinder, AR = 1). The lattice constant and layer separations are the same in both cases. The cases of cavity-free PDMS layers with the same overall thickness are plotted with and without loss for comparison.

IV. REFLECTION AND ABSORPTION

The relative importance of viscous vs reflection losses to the transmission reduction can be assessed by calculating the absorption loss (AL) in terms of the normalized reflected and transmitted intensities

$$AL = 1 - \frac{|P_{\text{trans}}(f)|^2}{|P_{\text{inc}}(f)|^2} - \frac{|P_{\text{ref}}(f)|^2}{|P_{\text{inc}}(f)|^2}. \quad (14)$$

Simulated transmission, reflection, and absorption results are plotted in Fig. 9 for the standard three-layer geometry considered experimentally. Comparison is made between the approximate-sphere and disk cases. Interestingly, more absorption is obtained in the resonant regime in the approximate-sphere case in contrast to what might be expected given the shear wave radiation discussed in Sec. II.

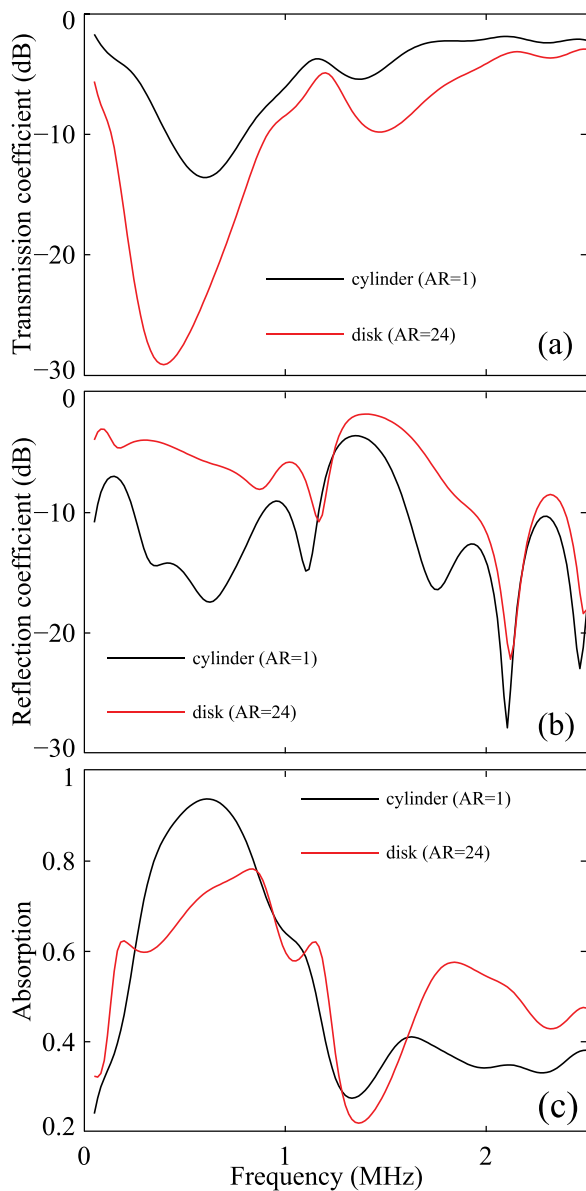


FIG. 9. (Color online) (a) Modeled transmission, (b) reflection, and (c) absorption dependence on cavity shape for the three-layer geometry. Cavity volume, lattice parameter, and layer thicknesses are held constant in both shape cases.

Calculation of the viscous dissipation field showed that although shear stress and absorption can be high around the corners of the disk, loss due to extensional strain throughout the volume immediately surrounding the $AR = 1$ cavity leads to a comparable order of magnitude of the total absorption in the two cases. In the higher frequency regime ($f > 1.5$ MHz), the trend appears to reverse with the disk layers having more absorption. It is important to note that an equivalent volume has been used as a basis for comparison. Other bases, such as equating the disk height to sphere radius, have the potential to show more absorption in the resonant regime in the higher AR case.¹¹

V. PARAMETER SENSITIVITY

Given the agreement between experimental and modeled results, it is reasonable to use modeling alone to determine transmission variation with primary geometric parameters such as disk tilt angle, layer thickness, and lattice constant. While exhaustive calculations are not pursued, large variations in the normal parameters considered in the experiment are modeled. This modeling is particularly useful to optimally reduce the overall layer thickness in comparison with the resonantly attenuated sound wavelength.

A. Transmission as a function of disk tilt angle

Although the volume fraction of air in the layers is small at 0.168%, the area-filling fraction of the disk is 12.6%. It is therefore useful to analyze how much of the performance is due to a resonant effect vs an area-based decoupling effect (incident wave encounters more reflective area).

As a test, the disk cavities are all uniformly rotated out-of-plane about their centers by 90° to minimize the area cross section that the incident field encounters. Results in Fig. 10 demonstrate a modest 5.2 dB reduction in transmission loss (relative to 27 dB) with this change, consistent with the picture that monopole resonance is primarily the cause of the transmission minimum. Moreover, inspection of the resonantly excited mode shape again revealed the breathing mode. Calculation of the reflection coefficient showed that

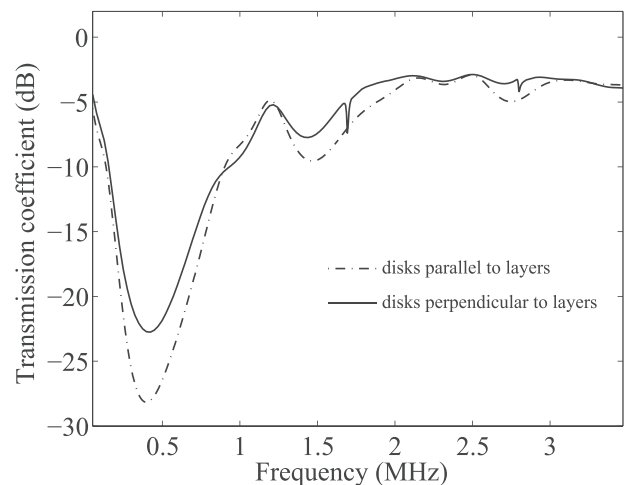


FIG. 10. Modeled transmission through a three-layer system of disk cavities for two different disk orientations.

near 400 kHz, reflected power reduced by 7% and absorbed power increased by 3%.

B. Variations with layer thickness

The advantage of low-frequency resonance is the ability to block sound of long wavelength relative to the scatterer size. Ideally, the overall layer thickness should also be small relative to a wavelength. The three-layer system studied experimentally achieved the 27 dB loss for a sound wavelength 2.5 times the overall layer thickness, which is relatively thick. Modeling is used to examine the possibility of reducing the overall layer thickness further in the three-layer system. Transmission changes for dividing d_z by two and eight are shown in Fig. 11. In the latter case, a maximum transmission loss of 18 dB is attained for a favorable sound wavelength 19 times the overall layer thickness.

Although it leads to thicker materials, d_z can be increased to create interference between the first Bragg resonance and the elastic monopole resonance of the cavities. Increasing d_z by a factor of 2 creates modest gain in transmission loss and shifts the minimum to lower frequency. Increasing d_z by a factor of 4 creates strong interference structure, however, the transmission minimum frequency does not lower significantly and the uniformity of transmission blocking suffers. Greater loss at the higher frequencies for the thicker cases is caused by the intrinsic compression wave absorption naturally through a thicker layer.

C. Variations with lattice constant and other parameters

Transmission loss results for halving the lattice constant d are shown in Fig. 12 for a single-layer array. Results can be compared with the normal case provided as a reference. A deep and wide transmission reduction is obtained indicative of a decoupling effect in contrast to a resonant effect. To provide perspective, the transmission loss caused by a $5\ \mu\text{m}$ planar air gap (limit of complete air filling in a unit cell) is also plotted. The gap, although impractical to

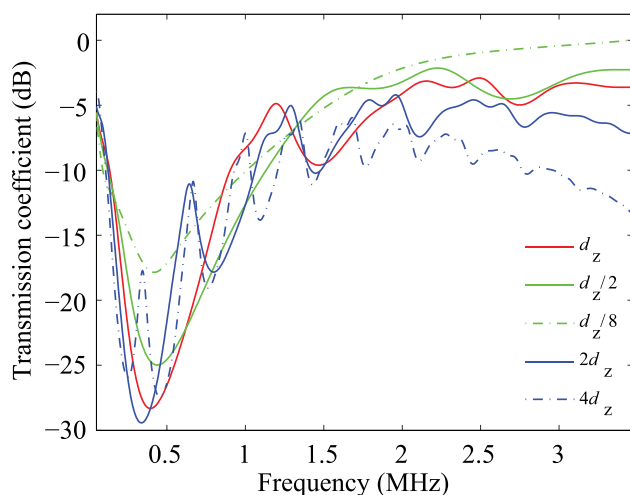


FIG. 11. (Color online) Modeled transmission for the three-layer case showing variation with decreasing or increasing layer separation parameter d_z (normal value = $375\ \mu\text{m}$).

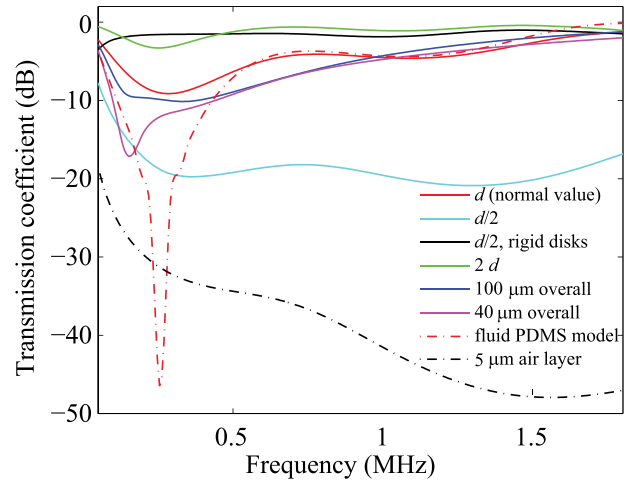


FIG. 12. (Color online) Modeled transmission through a single-layer disk array as a function of lattice constant (d) variation, disk compliance, overall layer thickness ($2d_z$), and elasticity of the layer. Normal value of the lattice constant is $d = 300\ \mu\text{m}$. The $5\ \mu\text{m}$ thick air layer case is the normal layer geometry, but with complete air filling of the cross section.

fabricate, produces a transmission loss $\gg 30\ \text{dB}$ over most frequencies.

The approximate stress-release boundary conditions on the cavity are essential as can be seen by modeling the contrasting case of rigid disks. Computing again for the halved lattice constant case, transmission loss is found to be very low. Separate results (not plotted) for the limiting lattice constant value of $120\ \mu\text{m}$ showed no more than 5 dB transmission loss over most of the frequency band considered. The gain in transmission compared to the previous cases is analogous to the superior acoustic-fluid radiation efficiency of low-frequency sound through rigid apertures compared to soft apertures.

Considering again the air-filled cavity, doubling the lattice constant weakens the resonant transmission blocking effect of the array, supporting the picture that the collective motion of the oscillators is important to obtain enough backscatter since a single cavity resonance in an unbounded medium is highly damped. The reduction in the resonant frequency toward the free-field value is also consistent with the previously noted influence of neighboring scatterers.

Along the lines of obtaining thin sound-blocking materials, results for reducing the overall thickness from $750\ \mu\text{m}$ down to $100\ \mu\text{m}$ or $40\ \mu\text{m}$ for the single-layer array case are plotted. The lattice constant is held at the normal value of $d = 300\ \mu\text{m}$. With a $40\ \mu\text{m}$ overall layer thickness, a noticeable decrease in the resonance frequency to 153 kHz is obtained at 17 dB loss, owing to the increasing compliance of the PDMS film covering the cavity. This transmission loss is obtained for a sound wavelength 243 times longer than the overall layer thickness.

Finally, the effect of replacing the elastic PDMS with an acoustic fluid model with the same density and sound speed is shown in the normal single-layer configuration. The deep minimum is caused by the assumed lack of viscous attenuation and shear elasticity of the fluid. The agreement of the minimum frequency with the elastic case is surprising in view of the fundamental difference in resonance between a simulated cavity in a soft medium and an air bubble in a

liquid. Specifically, separate computations showed that the monopole mode shape of a disk air bubble in an unbounded liquid does not appear drum-like, but instead a radial pulsation at the circumference is predominant. The resonant frequency of this bubble is 177 kHz. When located in the array, however, the lateral influence of neighboring cavities distorts the liquid displacement field into a field similar to the drum mode. This partly explains the fortuitous agreement, with the caveat that dominant restoring forces in the two oscillators are fundamentally different.

VI. CONCLUSIONS AND DISCUSSION

In underwater applications with constraints on thickness and allowable gas volume fraction due to buoyancy, the use of disk cavities for blocking sound transmission in thin materials offers an advantage over cavities that are approximately spherical since a larger reduction in transmission can be obtained at the lower frequencies for equivalent void fraction. Microscale soft lithography methods for sample fabrication provided an effective means of engineering variable cavity structure in acoustic materials that were examined by ultrasonic means. An analysis of the relative importance of absorption vs reflection to the transmission loss showed that near resonance the disk cavity arrays tend to be more reflective than absorptive in comparison with arrays of approximate spheres. At higher frequencies, this trend reverses with the disks being more absorptive.

For a single layer of disk cavities located mid-plane in a 40 μm overall thickness PDMS layer, a 17 dB modeled transmission loss was obtainable for a sound wavelength 243 times longer than the overall layer thickness. In the three-layer case, reducing the separation between layers tended to increase transmission over the measured and simulated standard configuration, although a 18 dB transmission loss was achievable for a sound wavelength about 20 times the overall layer thickness. In practice, a compromise between transmission blocking performance and hydrostatic pressure is needed to prevent cavity collapse (circular disk faces making contact). Clearly, the importance of this depends on the application. Using the finite element model developed for the disk cavity array, we performed an analysis of the hydrostatic problem, which predicted a 40% compression of cavity height (each circular surface deflecting by 1 μm) at 10 m depth in the three-layer experimental geometry. The depth for this deflection reduces to 6 m in the 40 μm thick single-layer case. These changes in hydrostatic pressure also impact the stiffness of the air cavities through the pressure dependent bulk modulus, so changes in transmission minimum frequencies would be expected.

ACKNOWLEDGMENTS

This research was supported by the Office of Naval Research.

¹F. G. Blake, Jr., "Spherical wave propagation in solid media," *J. Acoust. Soc. Am.* **24**, 211–215 (1952).

²D. V. Sivukhin, "Diffraction of plane sound waves by a spherical cavity," *Sov. Phys. Acoust.* **1**, 82–93 (1955).

- ³C. F. Ying and R. Truell, "Scattering of a plane longitudinal wave by a spherical obstacle in an isotropically elastic solid," *J. Appl. Phys.* **27**, 1086–1097 (1956).
- ⁴G. Gaunard, K. P. Scharnhort, and H. Überall, "Giant monopole resonances in the scattering of waves from gas-filled spherical cavities and bubbles," *J. Acoust. Soc. Am.* **65**, 573–594 (1979).
- ⁵V. N. Alekseev and S. A. Rybak, "Gas bubble oscillations in elastic media," *Acoust. Phys.* **45**, 535–540 (1999).
- ⁶E. Meyer, K. Brendel, and K. Tamm, "Pulsation oscillations of cavities in rubber," *J. Acoust. Soc. Am.* **30**, 1116–1124 (1958).
- ⁷M. Minnaert, "On musical air-bubbles and the sounds of running water," *Philos. Mag.* **16**, 235–248 (1933).
- ⁸B. Liang and J.-C. Cheng, "Acoustic localization in weakly compressible elastic medium containing air bubbles," *Phys. Rev. E* **75**, 016605 (2007).
- ⁹V. Leroy, A. Bretagne, M. Fink, H. Willaime, P. Tabeling, and A. Tourin, "Design and characterization of bubble phononic crystals," *Appl. Phys. Lett.* **95**, 171904 (2009).
- ¹⁰V. Leroy, A. Strybulevych, J. H. Page, and M. G. Scanlon, "Influence of positional correlations on the propagation of waves in a complex medium with polydisperse resonant scatterers," *Phys. Rev. E* **83**, 046605 (2011).
- ¹¹S. M. Ivansson, "Numerical design of Alberich anechoic coatings with superellipsoidal cavities of mixed sizes," *J. Acoust. Soc. Am.* **124**, 1974–1984 (2008).
- ¹²D. C. Calvo, A. L. Thangawng, and C. N. Layman, "Low-frequency resonance of an oblate spheroidal cavity in a soft elastic medium," *J. Acoust. Soc. Am.* **132**, EL1–EL7 (2012).
- ¹³K. M. Lee, P. S. Wilson, and M. S. Wochner, "Attenuation of standing waves in a large water tank using arrays of large tethered encapsulated bubbles," *J. Acoust. Soc. Am.* **135**, 1700–1708 (2014).
- ¹⁴I. N. Sneddon, "The distribution of stress in the neighborhood of a crack in an elastic solid," *Proc. R. Soc. London, Ser. A* **187**, 229–260 (1946).
- ¹⁵G. C. Sih and J. F. Loeber, "Normal compression and radial shear wave scattering at a penny-shaped crack in an elastic solid," *J. Acoust. Soc. Am.* **46**, 711–721 (1969).
- ¹⁶E. Domany, J. A. Krumhansl, and S. Teitel, "Quasistatic approximation to the scattering of elastic waves by a circular crack," *J. Appl. Phys.* **49**, 2599–2604 (1978).
- ¹⁷H. Oberst, "Resonant sound absorbers," in *Technical Aspects of Sound*, edited by E. G. Richardson (Elsevier, Amsterdam, 1957), Chap. 7, pp. 287–327.
- ¹⁸A.-C. Hladky-Hennion and J.-N. Decarpigny, "Analysis of the scattering of a plane acoustic wave by a doubly periodic structure using the finite element method: Application to Alberich anechoic coatings," *J. Acoust. Soc. Am.* **90**, 3356–3367 (1991).
- ¹⁹V. Leroy, A. Strybulevych, M. G. Scanlon, and J. H. Page, "Transmission of ultrasound through a single layer of bubbles," *Eur. Phys. J. E Soft Matter Biol. Phys.* **29**, 123–130 (2009).
- ²⁰COMSOL Multiphysics, version 4.4, <https://www.comsol.com/> (Last viewed 14 September 2014).
- ²¹P. C. Chou and N. J. Pagano, *Elasticity: Tensor, Dyadic, and Engineering Approaches* (Dover, New York, 1992), pp. 60–62.
- ²²G. Gaunard, "One-dimensional model for acoustic absorption in a viscoelastic medium containing short cylindrical cavities," *J. Acoust. Soc. Am.* **62**, 298–307 (1977).
- ²³R. Lane, "Absorption mechanisms for waterborne sound in Alberich anechoic layers," *Ultrasonics* **19**, 28–30 (1981).
- ²⁴G. Gaunard, "Comments on absorption mechanisms for waterborne sound in Alberich anechoic layers," *Ultrasonics* **23**, 90–91 (1985).
- ²⁵V. Easwaran and M. L. Munjal, "Analysis of reflection characteristics of a normal incidence plane wave on resonant sound absorbers: A finite element approach," *J. Acoust. Soc. Am.* **93**, 1308–1318 (1993).
- ²⁶J. E. Gubernatis, E. Domany, and J. A. Krumhansl, "Formal aspects of the theory of the scattering of ultrasound by flaws in elastic materials," *J. Appl. Phys.* **48**, 2804–2811 (1977).
- ²⁷R. Lim and R. H. Hackman, "Comments on the calculation of cross sections for elastic-wave scattering using the T matrix," *J. Acoust. Soc. Am.* **87**, 1070–1075 (1990).
- ²⁸A. D. Pierce, *Acoustics. An Introduction to Its Physical Principles and Applications* (AIP, Melville, NY, 1989), p. 220, Eq. (5-3.10).
- ²⁹P. Y. Longin, C. Verdier, and M. Piau, "Dynamic shear rheology of high molecular weight polydimethylsiloxanes: Comparison of rheometry and ultrasound," *J. Non-Newtonian Fluid Mech.* **76**, 213–232 (1998).

³⁰A. J. Romano, J. A. Bucaro, B. H. Houston, J. L. Kugel, P. J. Rossman, R. C. Grimm, and R. L. Ehman, "On the feasibility of elastic wave visualization within polymeric solids using magnetic resonance elastography," *J. Acoust. Soc. Am.* **116**, 125–132 (2004).

³¹W. Sachse and Y. H. Pao, "On the determination of phase and group velocities of dispersive waves in solids," *J. Appl. Phys.* **49**, 4320–4327 (1978).

³²G. R. Fowles, *Introduction to Modern Optics* (Dover, New York, 1989), p. 94, Eq. (4.16).